Chemical stability of Li_4PS_4I solid electrolyte against hydrolysis

Marcela Calpa[a], Nataly Carolina Rosero-Navarro[b*], Akira Miura[b], Randy Jalem[c,d,e], Yoshitaka Tateyama[c,e] and Kiyoharu Tadanaga[b]

[a.] Graduate School of Chemical Sciences and Engineering, Hokkaido University, Sapporo 060-8628, Japan

[b.] Division of Applied Chemistry, Faculty of Engineering, Hokkaido University, Sapporo 060-8628, Japan

[c.] Center for Green Research on Energy and Environmental Materials (GREEN), National Institute for Materials Science (NIMS), Tsukuba, Ibaraki 305-0044, Japan

[d.] PRESTO, Japan Science and Technology Agency (JST), Saitama 333-0012, Japan

[e.] Elements Strategy Initiative for Catalysts & Batteries, Kyoto University, Kyoto, Kyoto 615-8245, Japan

* corresponding author: rosero@eng.hokudai.ac.jp

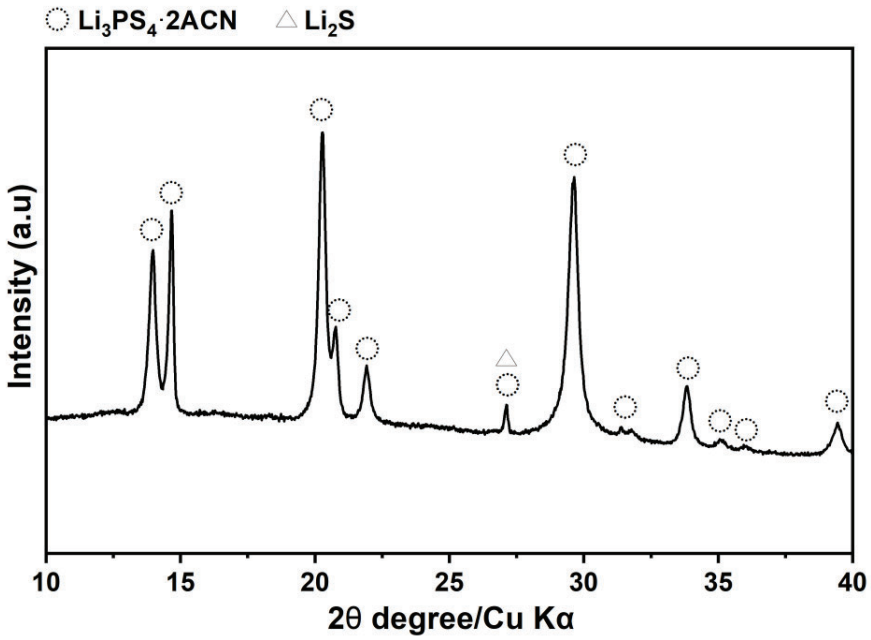

Figure S1. XRD pattern of $Li_3PS_4 \cdot 2ACN$ [1].

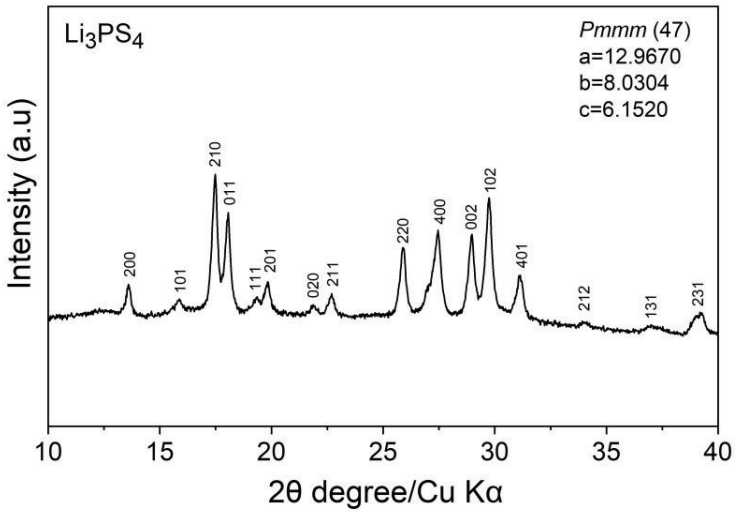

Figure S2. Indexed XRD pattern of the Li_3PS_4 sample.

Table S1. Cell parameters of the Li_3PS_4 sample

a (Å)	12.9670
b (Å)	8.0304
c (Å)	6.1520
α (°)	90
β (°)	90
ɤ (°)	90
Volume ($Å^3$)	640.618
Space group	*Pmmm*(47)

Figure S2 and Table S1 shows Indexed XRD pattern and cell parameters of the Li_3PS_4 sample. The cell parameters of the Li_3PS_4 sample are in good agreement with those reported for β-Li_3PS_4 crystal phase [2].

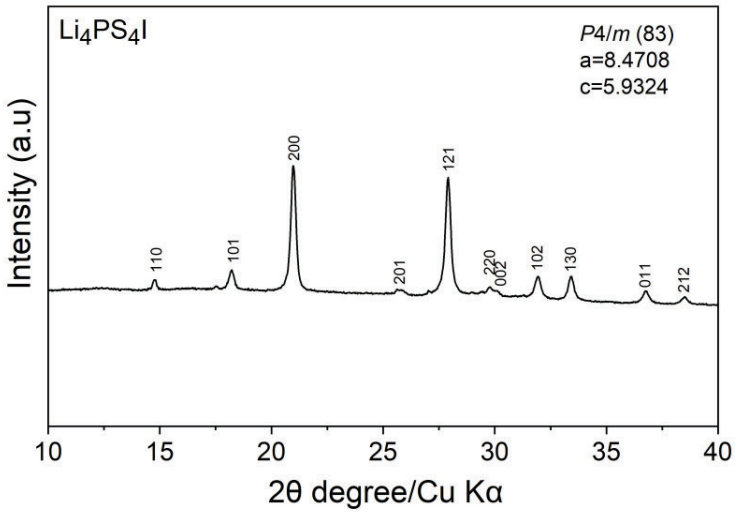

Figure S3. Indexed XRD pattern of the Li_3PS_4·1LiI sample.

Table S2. Cell parameters of the Li_3PS_4·1LiI sample

a (Å)	8.4708
b (Å)	8.4708
c (Å)	5.9324
α (°)	90
β (°)	90
ɤ (°)	90
Volume ($Å^3$)	425.681
Space group	*P*4/*m*(83)

Figure S3 and Table S2 shows indexed XRD pattern and cell parameters of the Li_3PS_4·1LiI sample. The cell parameters of the Li_3PS_4·1LiI sample are in good agreement with those reported for the Li_4PS_4I crystal phase [3].

More detailed studies on the crystal structures of β-Li_3PS_4 and Li_4PS_4I are reported by Stöffler et al. [2] and Sedlmaier et al [3], respectively. Table S3 shows the comparison of the cell parameters between β-Li_3PS_4 and Li_4PS_4I:

Table S3. Cell parameters of β-Li_3PS_4 and Li_4PS_4I

Cell parameters	β-Li_3PS_4 [2]	Li_4PS_4I [3]
a (Å)	12.993	8.48284
b (Å)	8.0458	8.48284
c (Å)	6.1377	5.93013
α (°)	90	90
β (°)	90	90
ɤ (°)	90	90
Volume ($Å^3$)	641.6(2)	426.725(15)
Space group	Pnma(62)	P4/nmm

In the crystal structure of Li_4PS_4I, the arrangement of the PS_4^{3-} tetrahedra and their orientation look similar to the one in α-Li_3PS_4, the high-temperature polymorph of Li_3PS_4, with every second PS_4^{3-} tetrahedron replaced by I^- [3]. Thus, the incorporation of LiI into Li_3PS_4 results in the formation of a different PS_4 tetrahedral framework of that in β-Li_3PS_4.

Table S4. Ionic conductivity at room temperature, activation energy and density of pelletized $Li_3PS_4 \cdot xLiI$ samples with x=0, 0.5, 1 and 1.5.

Sample	σ_{RT} (S cm^{-1})	Room temperature	E_a (kJ mol^{-1})	ρ_{pellet} (g cm^{-3})
Li_3PS_4	$5.1x10^{-5}$	19 °C	9.78	1.68
$Li_3PS_4 \cdot 0.5LiI$	$1.5x10^{-4}$	19 °C	12.04	1.81
$Li_3PS_4 \cdot 1LiI$	$1.3x10^{-4}$	19 °C	12.04	1.56
$Li_3PS_4 \cdot 1.5LiI$	$9.2x10^{-5}$	24 °C	19.31	1.9

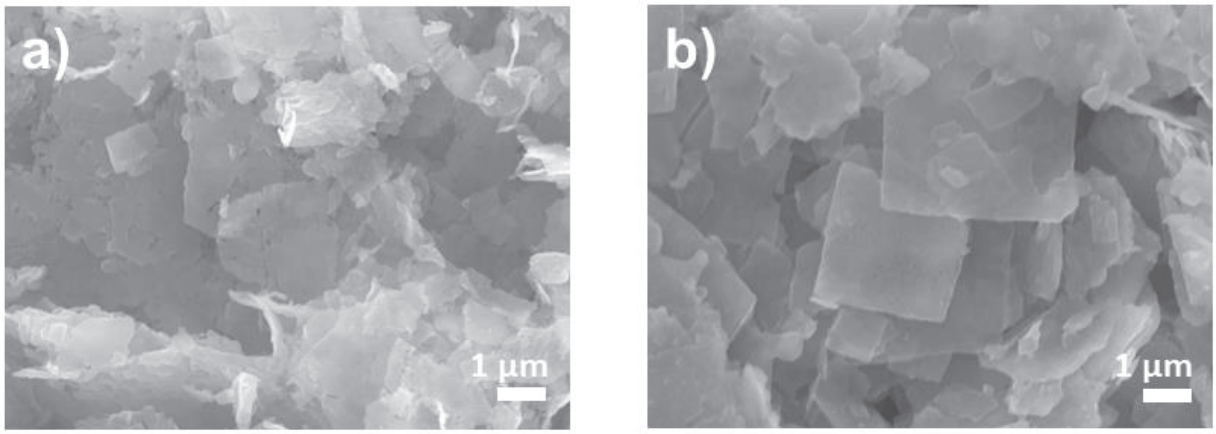

Figure S4. SEM images of the a) Li_3PS_4 and b) Li_4PS_4I solid electrolytes.

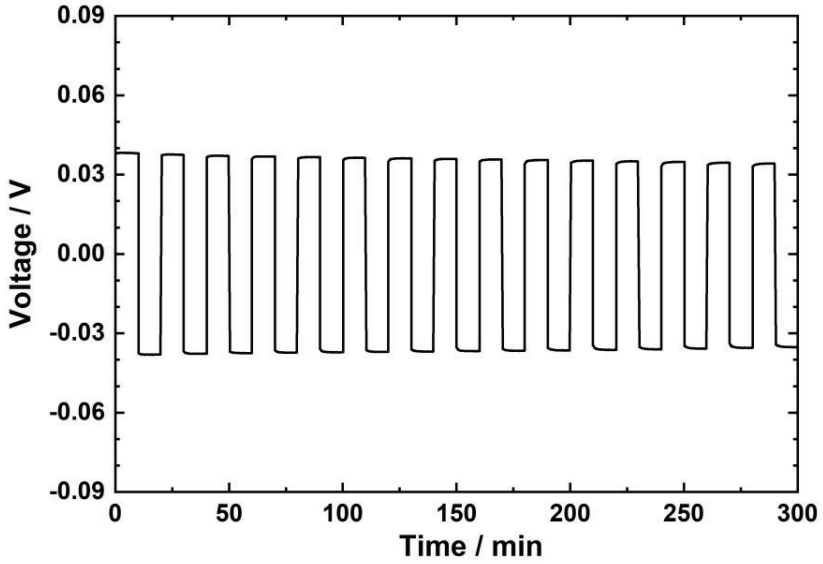

Figure S5. Direct current (DC) cycling of a Li/Li_4PS_4I/Li cell.

A symmetric Li/Li_4PS_4I/Li cell was fabricated and cycled at a current density of 0.1 mA cm^{-2}, at room temperature. A slightly reduction on the interfacial resistance is observed with time. It is assigned to the formation of a more homogeneous Li layer with cycling. The successful cycling of the Li/Li_4PS_4I/Li cell demonstrates the good interfacial stability of Li_4PS_4I with Li metal.

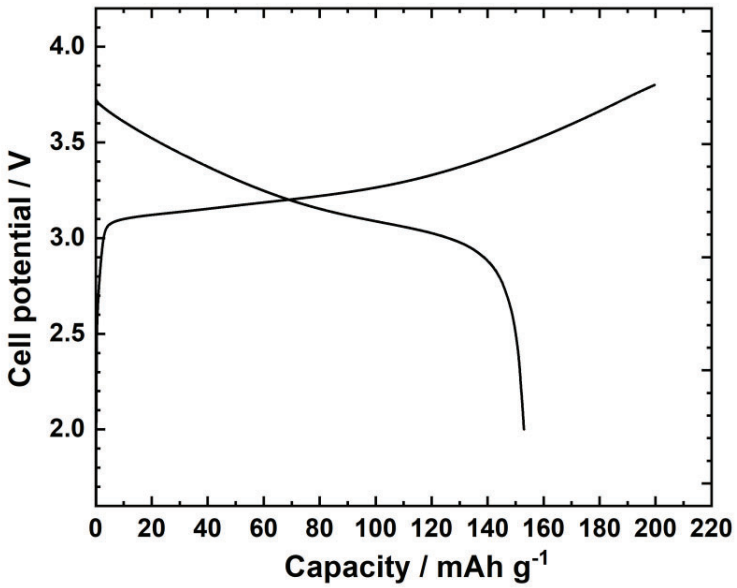

Figure S6. First charge-discharge curve of an all-solid-state cell using $LiNi_{1/3}Co_{1/3}Mn_{1/3}O_2$ (NCM) as active material, Li_4PS_4I as the ionic conductor and Vapor Grown Carbon Fiber (VGCF) as the electronic conductor in the composite cathode. The weight ratio was 69:29:2, respectively. The all-solid-state battery was constructed as reported elsewhere[4]. Charge-discharge measurements were conducted using a constant current (CC) mode at a current density of 0.13 MA cm^{-2} and cut-off voltages of 3.8 and 2 V.

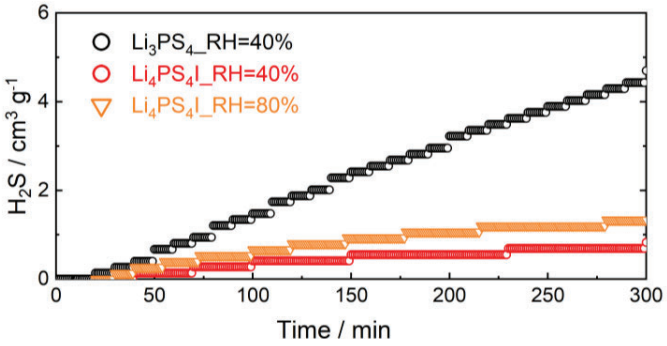

Figures S7. H_2S gas generation from the Li_4PS_4I sample under relative humidity of 40% (red) and 80% (orange). The H_2S gas generation from the Li_3PS_4 sample under relative humidity of 40% (black) is included for comparison. All measurements were carried out at 20 °C.

Measurements under relative humidity of 40% were carried out as described in the experimental section, the pelletized sample and an H_2S gas sensor (ToxiRAE Pro PGM-1860) were placed in a closed 2000 cm^3 desiccator in air and the H_2S concentration was measured by the gas sensor. For measurements under relative humidity of 80%, the desiccator was placed in a humidity chamber (Yamato iw211) set at 80% relative humidity and 20 °C prior the measurement.

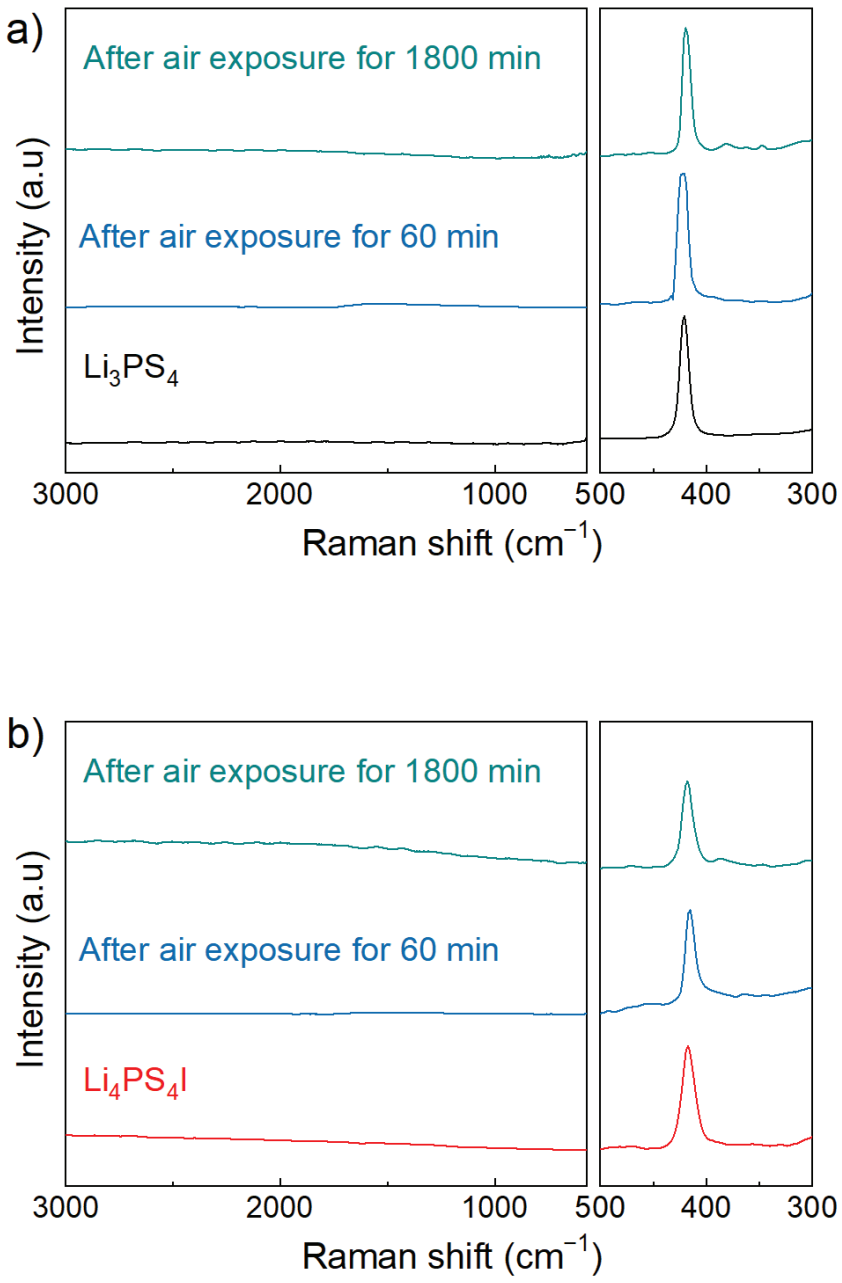

Figure S8. Raman spectra of a) Li_3PS_4 and b) Li_4PS_4I samples prior to and after exposure to the ambient atmosphere for 60 min and 1800 min.

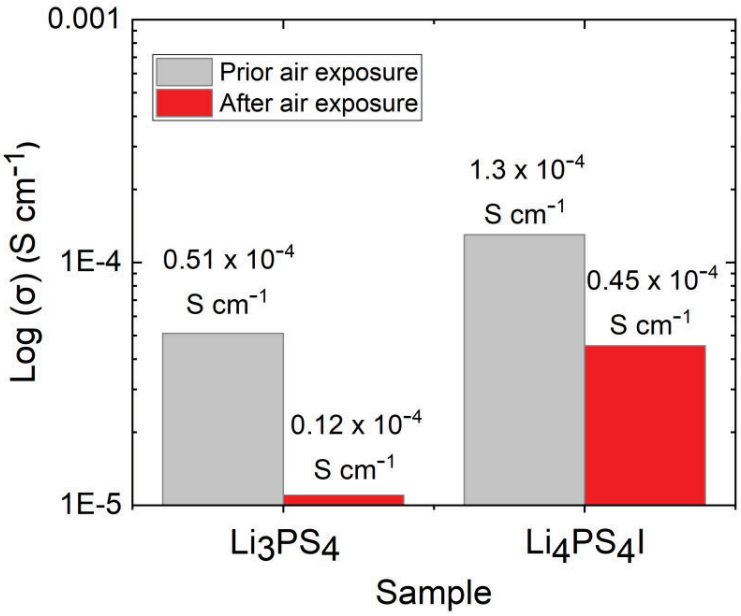

Figure S9. Ionic conductivity of Li_3PS_4 and Li_4PS_4I solid electrolytes prior and after exposure to the ambient atmosphere for 60 min.

Reactions of Li_3PO_4 towards H_2O calculated by DFT

$16Li_3PO_4 + H_2O \rightarrow Li_{47}HP_{16}O_{64} + LiOH$, ΔH (cal) =−0.62 eV (s1)

$32Li_3PO_4 + H_2O \rightarrow 2Li_{47}P_{16}HO_{64} + Li_2O$, ΔH (cal) =−0.49 eV (s2)

Reactions s1 and s2 relate to the reaction of Li_3PO_4 with H_2O. When in contact with H_2O, Li_3PO_4 is determined to have $\Delta H < 0$ for protonation reaction. This is indicative that if Li_3PO_4 forms in a Li_3PS_4 sample at the initial stage of the hydration process at the surface or grain boundary region, it continues to capture protons spontaneously. Subsequent reactions result in the formation of side phases such as LiOH and Li_2O. The unknown peaks observed in the XRD patterns of the Li_3PS_4 sample after exposure to the ambient atmosphere (Figure 4a) may be assigned to the decomposition products of Li_3PO_4. Moreover, formation of LiOH and Li_2O could explain the easy fragmentation (into side phases) observed in the Li_3PS_4 sample exposed to the ambient atmosphere (Figure 3c).

References

1. H. Wang, Z. D. Hood, Y. N. Xia and C. D. Liang, *J. Mater. Chem. A*, 2016, **4**, 8091-8096.
2. H. Stöffler, T. Zinkevich, M. Yavuz, A. Senyshyn, J. r. Kulisch, P. Hartmann, T. Adermann, S. Randau, F. H. Richter and J. r. Janek, *The Journal of Physical Chemistry C*, 2018, **122**, 15954-15965.
3. S. J. Sedlmaier, S. Indris, C. Dietrich, M. Yavuz, C. Dräger, F. von Seggern, H. Sommer and J. r. Janek, *Chem. Mater.*, 2017, **29**, 1830-1835.
4. M. Calpa, N. C. Rosero-Navarro, A. Miura and K. Tadanaga, *Electrochim. Acta*, 2019, **296**, 473-480.